mass,[12] all three events have a K^+ produced at the production vertex and furthermore, the invariant mass recoiling off the K^+ is approximately the same in all three events. For Events I, II, and III, the mass recoiling off the K^+ is 2.73, 2.70, and 2.76 GeV/c^2, respectively. We have also observed that the first Ω^- reported by Brookhaven and the Ω^- reported by the British-Munich collaboration were both produced in the reaction $K^-+p\rightarrow\Omega^-+K^++K^0$. The invariant mass recoiling off the K^+ for these events is 2.69 and 2.68 GeV/c^2, respectively. This suggests that perhaps Ω^- hyperons are produced in the decay of an $S=-2$ particle of mass $\sim$2720 MeV/c^2. We hasten to point out, however, that at 5.5-GeV/c K^- beam momentum, phase space has its maximum at 2.50 GeV/c^2 for the Ω^-K^0 combination and at 2.70 GeV/c^2 for the Ω^-K^{*0} combination. Thus, it would be interesting to look at the invariant mass combinations in Ω^- events produced with higher K^- beam momenta.

[12] The π^+ interpretation requires two missing K^0's in order to conserve strangeness and the available invariant mass of 1.023 $\pm$0.056 GeV/c^2 for this interpretation indicates the two K^0's are produced with approximately the same momentum and direction. This would seem to be an improbable situation. On the other hand, if track 2 is assumed to be a K^+, the missing mass at the production vertex is 0.898 GeV/c^2, close to the mass of the K^*(890) resonance. Hence we expect the correct interpretation of track 2 to be a K^+ rather than a π^+.

ACKNOWLEDGMENTS

We wish to express our appreciation and gratitude to the members of the ZGS and MURA bubble-chamber crews for their cooperation and patience in obtaining the film for this experiment. We also gratefully acknowledge the efforts of many others in the scanning, measuring, and analysis of these events.

PHYSICAL REVIEW VOLUME 168, NUMBER 5 25 APRIL 1968

Differential Pion Charge-Exchange Scattering and η Production: $\pi^-+p\rightarrow\pi^0+n$ from 2.4 to 3.8 GeV/c, at 6 GeV/c, and at 10 GeV/c; $\pi^-+p\rightarrow\eta^0+n$ at 10 GeV/c†

M. A. WAHLIG*
Laboratory for Nuclear Science, Massachusetts Institute of Technology, Cambridge, Massachusetts

AND

I. MANNELLI
Istituto di Fisica, dell'Università di Pisa,
and
Istituto Nazionale di Fisica Nucleare, Sezione di Pisa, Pisa, Italy
(Received 13 October 1967)

Small-angle differential cross sections are presented here for $\pi^-+p\rightarrow\pi^0+n$ charge-exchange scattering between 2.4 and 3.8 GeV/c. The differential cross section near $t=0$ displays two minima and one maximum in this momentum interval, reflecting the presence of the $N_{3/2}^*(2420)$, $N_{3/2}^*(2850)$, and $N_{1/2}^*(2650)$ resonances; at larger t values, the cross sections fall off exponentially as a function of t, just as has been previously observed for charge-exchange scattering above 6 GeV/c. The pion-charge-exchange data reported here at 6 and 10 GeV/c extend out to large angles, showing a maximum near $t=0$, followed by an exponential falloff as e^{10t}, a minimum near $-t=0.6$ (GeV/c)^2, and then a second maximum near $-t=1.0$ (GeV/c)^2. The $\pi^-+p\rightarrow\eta^0+n$ differential cross section shows a maximum near $t=0$, followed by an exponential falloff as e^{4t}, much less steep than the π^0 slope. These data are compared to our previously published data and to those of the Saclay-Orsay group.

I. INTRODUCTION

IN an experiment at the AGS at Brookhaven National Laboratory, we studied the interaction $\pi^-+p\rightarrow n$ plus γ's in several experimental setups, resulting in measurements of the following final states: (A) $n+2\gamma$ in a low-momentum π^- beam covering the range of 2.4 to 3.8 GeV/c in steps of 0.1 GeV/c, plus one point at 6.0 GeV/c; (B) $n+2\gamma$ in a high-momentum π^- beam covering the range of 6 to 16 GeV/c, with a "good-geometry" measurement (spark chamber far downstream from hydrogen target); (C) $n+2\gamma$, $n+3\gamma$, $n+4\gamma$ in the same high-momentum π^- beam, at 10 GeV/c only, with a "poor-geometry" measurement (spark chamber close to hydrogen target).

We report here the results of measurement (A), in which we observe the charge-exchange $n+\pi^0$ final state only, and the $n+2\gamma$ results of measurement (C), in which we observe both the $n+\pi^0$ and $n+\eta^0$ final states. Preliminary results of the forward charge-

† Work supported in part through funds provided by the U. S. Atomic Energy Commission under Contract AT(30-1)-2098. This research was performed, using the alternating gradient synchrotron at Brookhaven National Laboratory.
* Present address: Lawrence Radiation Laboratory, University of California, Berkeley, California.

exchange scattering from (A) have already been reported,[1] as have some of the $n+2\gamma$ results from (C).[2,3] The final results of (B)[4] and the final results of the 3γ [5] and 4γ [6,3] final states of (C) have been reported previously.

These 13 measurements in the momentum region between 2.4 and 3.8 GeV/c represent a systematic extension of the charge-exchange scattering measured by Bulos *et al.*[7] up to 1.1 GeV, by Chiu *et al.*[8] up to 1.3 GeV, and by Borgeaud *et al.*[9] up to 1.9 GeV. Stirling *et al.*[10] and Sonderegger *et al.*[11] published charge-exchange scattering in the 5.9- to 18.2-GeV/c momentum range; their results and ours of Refs. 4 and 2 are in excellent agreement with each other. This same group will soon publish charge-exchange results for the momentum range 2.6 to 5.8 GeV/c. Additional data in the momentum range 1.3 to 4.0 GeV/c have also been taken by the group of Ref. 7.[12] In addition, Carroll *et al.*[13] have measured the charge-exchange reaction at five momenta between 1.72 and 2.46 GeV/c. In Refs. 7, 8, 12, and 13, differential measurements have been made over the complete angular range, whereas our data and those of the Saclay-Orsay group in Refs. 9–11 have been limited to scattering angles near the forward direction. Charge-exchange distributions have also been measured by Faissner *et al.*[14] at 4.0 GeV/c, by Barmin *et al.*[15] at 2.8 GeV/c, and by Backenstoss *et al.*[16] at 10 GeV/c.

η production in the reaction $\pi^- + p \rightarrow \eta^0 + n$ has been measured between 3 and 18 GeV/c by the Saclay-Orsay group, Guisan *et al.*,[17] and it has been interpreted in the framework of a single Regge-pole exchange by Phillips and Rarita.[18]

The type of interpretation of charge-exchange scattering varies as a function of the incident pion momentum in much the same way as does elastic scattering. At low momenta, $\lesssim 1.5$ GeV/c, the angular distributions are expanded in partial waves[7,8] in order to obtain additional information on the pion-nucleon phase shifts and on the quantum numbers of the pion-nucleon resonances. At high momenta, the differential distributions, in terms of the square of the four-momentum transfer t, are compared with the predictions of peripheral-type production models, in particular, the Regge-pole theory,[19–21] the absorption model,[22] and the Byers-Yang "coherent-droplet" model.[23] The single Regge-pole exchange model adequately explains the energy dependence of these distributions and provides an adequate parametrization (although not an explanation) of the t dependence. The coherent-droplet model explains the t dependence of the charge-exchange distributions [for $|t| \lesssim 0.5$ (GeV/c)^2] and inserts the energy dependence in the form of a normalization parameter.

At intermediate momenta, $\sim$1.5 to 6 GeV/c, a combination of the effects of direct-channel resonances and of a cross-channel exchange interaction is necessary to explain the data, but the high spin values of the resonances in this energy region make it difficult to obtain unique fits to the data. However, it appears that, with reasonable choices of the spins of the resonances, the parities of the resonances may be determined. This type of analysis, using direct-channel resonance plus Regge-pole exchange amplitudes, has been carried out, using charge-exchange data, by Carroll *et al.*[13] near 2 GeV/c and by Baacke and Yvert[24] between 2.6 and 5.8 GeV/c. Barger and Olsson[25] have applied the same type of analysis to the 0° charge-exchange data between 0.7 and 6.0 GeV/c.

[1] M. A. Wahlig, I. Mannelli, L. Sodickson, O. Fackler, C. Ward, T. Kan, and E. Shibata, Phys. Rev. Letters **13**, 103 (1964).

[2] M. A. Wahlig, I. Mannelli, L. Sodickson, O. Fackler, C. Ward, T. Kan, E. Shibata, and D. Frisch, in *Proceedings of the Twelfth Annual Conference on High-Energy Physics, Dubna, 1964* (Atomizdat, Moscow, 1965), p. 115.

[3] M. A. Wahlig, E. Shibata, and I. Mannelli, Phys. Rev. Letters **17**, 221 (1966).

[4] I. Mannelli, A. Bigi, R. Carrara, M. Wahlig, and L. Sodickson, Phys. Rev. Letters **14**, 408 (1965).

[5] E. Shibata and M. Wahlig, Phys. Letters **22**, 354 (1966).

[6] M. Wahlig, E. Shibata, D. Gordon, D. Frisch, and I. Mannelli, Phys. Rev. **147**, 941 (1966). The results reported in this reference include the preliminary data reported earlier by L. Sodickson, M. Wahlig, I. Mannelli, D. Frisch, and O. Fackler, Phys. Rev. Letters **12**, 485 (1964).

[7] F. Bulos *et al.*, Phys. Rev. Letters **13**, 558 (1964).

[8] C. B. Chiu, R. D. Eandi, A. C. Helmholz, R. W. Kenney, B. J. Moyer, J. A. Poirier, W. B. Richards, R. J. Cence, V. Z. Peterson, N. K. Sehgal, and V. J. Stenger, Phys. Rev. **156**, 1415 (1967).

[9] P. Borgeaud, C. Bruneton, Y. Ducros, P. Falk-Vairant, O. Guisan, J. Movchet, P. Sonderegger, A. Stirling, M. Yvert, A. Tran Ha, and S. D. Warshaw, Phys. Letters **10**, 134 (1964).

[10] A. V. Stirling, P. Sonderegger, J. Kirz, P. Falk-Vairant, O. Guisan, C. Bruneton, P. Borgeaud, M. Yvert, J. P. Guillaud, C. Caverzasio, and B. Amblard, Phys. Rev. Letters **14**, 763 (1965).

[11] P. Sonderegger, J. Kirz, O. Guisan, P. Falk-Vairant, C. Bruneton, P. Borgeaud, A. V. Stirling, C. Caverzasio, J. P. Guillaud, M. Yvert, and B. Amblard, Phys. Letters **20**, 75 (1966).

[12] Some of these data have already been analyzed in unpublished theses: Bennet B. Brabson, MIT, 1966, and Albert E. Pifer, Brown University, 1967.

[13] A. S. Carroll, I. F. Corbett, C. J. S. Damerell, N. Middlemas, D. Newton, A. B. Clegg, and W. S. C. Williams, Phys. Rev. Letters **16**, 288 (1966).

[14] H. Faissner, F. Ferrero, H. J. Gerber, M. Reinharz, and J. Stein, Phys. Letters **11**, 178 (1964).

[15] V. V. Barmin, A. G. Dolgolenko, A. G. Meshkovsky, and V. A. Shebanov, Report No. 401, Institute for Theoretical and Experimental Physics, Moscow, 1965 (unpublished).

[16] G. Backenstoss, B. Hyams, W. Männer, A. Reale, and U. Stierlin, Nuovo Cimento **42**, 814 (1966).

[17] O. Guisan, J. Kirz, P. Sonderegger, A. V. Stirling, P. Borgeaud, C. Bruneton, P. Falk-Vairant, B. Amblard, C. Caverzasio, J. P. Guillaud, and M. Yvert, Phys. Letters **18**, 200 (1965).

[18] Roger J. N. Phillips and William Rarita, Phys. Rev. Letters **15**, 807 (1965); Phys. Rev. **140**, B200 (1965).

[19] Robert K. Logan, Phys. Rev. Letters **14**, 414 (1965).

[20] Roger J. N. Phillips and William Rarita, Phys. Rev. **139**, B1336 (1965).

[21] G. Höhler, J. Baacke, H. Schlaile, and P. Sonderegger, Phys. Letters **20**, 79 (1966).

[22] E. M. Henley and I. J. Muzinich, Phys. Rev. **136**, B1783 (1964).

[23] N. Byers and C. N. Yang, Phys. Rev. **142**, 976 (1966).

[24] J. Baacke and M. Yvert, in *Proceedings of the Thirteenth Annual International Conference on High-Energy Physics, Berkeley, California, 1966* (University of California Press, Berkeley, Calif., 1967); Nuovo Cimento **51A**, 761 (1967).

[25] V. Barger and M. Olsson, Phys. Rev. **151**, 1123 (1966).

On the other hand, the 0° values of the differential cross section are very useful throughout all momentum regions as an experimental check on dispersion-relation calculations.[26,27] This can be seen using the relationship between the complex charge-exchange amplitude F_{ex} and the amplitudes for π^+p and π^-p elastic scattering $F_\pm$,

$$\sqrt{2}F_{\text{ex}}=(F_+-F_-)\,, \tag{1}$$

together with the optical theorem

$$4\pi\,\text{Im}F_\pm(0°)=k\sigma^\pm\,, \tag{2}$$

where $\sigma^\pm$ are the π^+p and π^-p total cross sections, and k is the pion momentum. Combining these,

$$\sqrt{2}F_{\text{ex}}(0°)=(D_+-D_-)+ik(\sigma^+-\sigma^-)/4\pi\,, \tag{3}$$

where $D_\pm$ are the real parts of the $\pi^\pm p$ scattering amplitudes at 0°. By measuring $d\sigma_{\text{ex}}/d\Omega(0°)=|F_{\text{ex}}(0°)|^2$ and the $\pi^\pm p$ total cross sections, (D_+-D_-) can be determined experimentally, and then compared with the dispersion-relation calculation of (D_+-D_-).

In intermediate momentum regions, the pion-nucleon resonances produce only small increases in the total cross sections, but the $\pi^\pm p$ total cross sections are nearly equal, so that the resonances produce relatively large effects on their difference. Structure in the energy dependence of $d\sigma_{\text{ex}}/d\Omega(0°)$ can therefore be a much more sensitive indication of the presence of pion-nucleon resonances than total cross-section measurements. This was indicated in our preliminary results,[1] which showed the effects of two additional resonances above the $N_{3/2}^*(2420)$ resonance. These were subsequently confirmed by precision total cross-section measurements[28] as the $N_{1/2}^*(2650)$ and $N_{3/2}^*(2850)$ resonances. However, these amplitudes have non-negligible real parts, and so, in general, the maximum or minimum in the charge-exchange forward cross section does not occur at exactly the same energy as does the peak in the $\pi^\pm p$ total cross section.

II. EXPERIMENT

A. Low-Energy Run

The experimental apparatus is shown in Fig. 1. The 2.4- to 6.0-GeV/c π^- beam enters from the left. The spread in momentum was ±0.4%. No Čerenkov counter was used, so corrections are made for μ^-- and K^--beam contamination. The incident beam was defined by three scintillation counters not shown in Fig. 1 plus the $\frac{1}{16}$-in.-thick scintillator immediately in front of the hydrogen target.

The 2-in.-long hydrogen target was surrounded by alternate layers of scintillating plastic and lead (Pb),

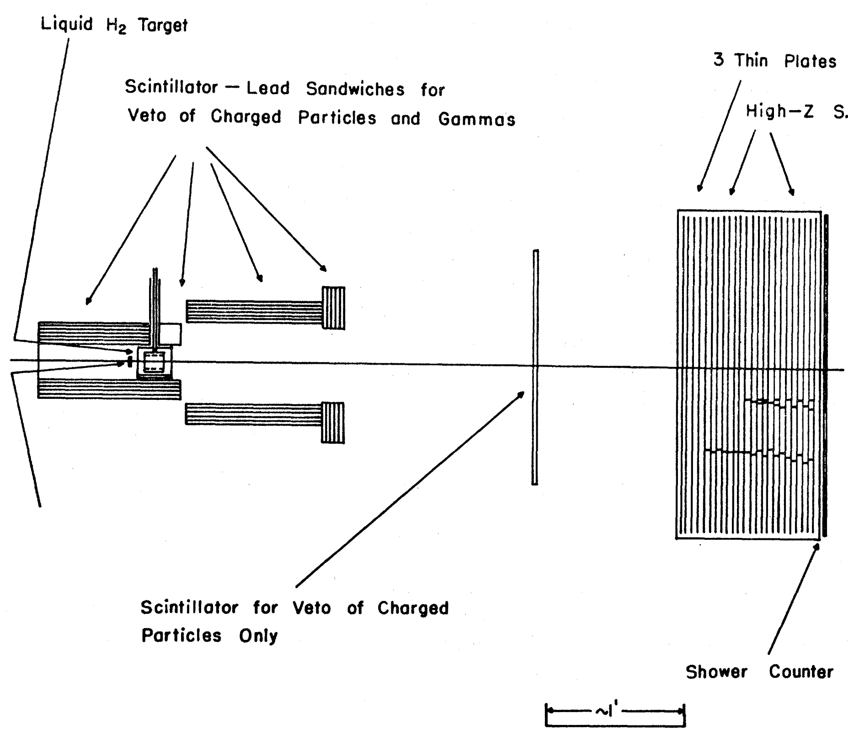

FIG. 1. Schematic of experimental apparatus.

[26] B. Amblard, P. Borgeaud, Y. Ducros, P. Falk-Vairant, O. Guisan, W. Laskar, P. Sonderegger, A. Stirling, M. Yvert, A. Tran Ha, and S. D. Warshaw, Phys. Letters **10**, 138 (1964).
[27] G. Höhler, J. Baacke, and R. Strauss, Phys. Letters **21**, 223 (1966).
[28] W. Galbraith, Proc. Roy. Soc. (London) **A289**, 521 (1966); A. Citron, W. Galbraith, T. F. Kycia, B. A. Leontic, R. H. Phillips, A. Rousset, and P. H. Sharp, Phys. Rev. **144**, 1101 (1966).

except for the upstream and downstream directions and a small hole to admit the liquid hydrogen. There were three layers of $\frac{1}{2}$-in. scintillator and two layers of $\frac{1}{2}$-in. lead. These scintillator-lead sandwiches were in anticoincidence with the incident beam and vetoed both charged particles and γ's, except those in the downstream direction (at these momenta, the upstream hole in this counter system was neglected).

The square opening in the downstream direction, subtending approximately $12°\times12°$ in the lab, was covered only by a $\frac{1}{2}$-in.-thick scintillator, which vetoed only charged particles. γ rays passed through this scintillator and were converted in a 14-plate brass spark chamber 5 radiation lengths thick. The detection of one or more charged particles in a large scintillation counter directly downstream from the spark chamber completed the trigger; this shower detector had a 4-in.-square hole in its center to avoid overloading by beam particles. The spark chamber had an additional three plates of thin aluminum foil on the upstream side to provide a visual veto of any charged particles which escaped our veto system. The spark-chamber plates were $25\times25\times\frac{1}{4}$ in. thick, and the first brass plate was $60\pm\frac{1}{4}$ in. from the center of the hydrogen target.

The incident beam intensity was typically (1.0 to 1.5) $\times10^4$ particles per 100-msec-long pulse. A dead-time circuit was used to turn off the electronics for 0.8 μsec each time a charged particle traversed the spark chamber to lower the probability of a charged-particle track accompanying the charge-exchange event. The fraction of the incident beam intensity eliminated by this dead-time protection varied between $\frac{1}{4}$ and $\frac{3}{4}$, usually closer to the latter. With this dead-time circuitry, 28% of the 2γ events were accompanied by a single charged track and 6% by two charged tracks. Those events with three or more charged tracks were not measured, but were corrected for in the normalization.

The spark-chamber trigger rate was typically about 1.1×10^{-4} trigger per incident particle with the target full and about 0.55×10^{-4} with the target empty. Between 5000 and 10 000 pictures were taken at each of the 14 momenta, and about one half of these contained 2γ events.

B. Poor-Geometry High-Energy Run

The 10-GeV/c data reported here were taken in a beam originally set up by Galbraith *et al.*[29] and included a differential Čerenkov counter to discriminate against K^- and $\bar{p}$. The momentum spread was $\pm2\%$ at half-height of a triangular distribution, and the angular divergence was smaller than 2 mrad.

The experimental arrangement was the same as that used in the low-energy beam, with three exceptions: The length of the hydrogen target was increased to 6 in., the large scintillation counter downstream from the spark chamber was not used, and the hydrogen-target-to-spark-chamber distance was decreased to 47 in. (This should not be confused with the good-geometry high-energy data at 10 GeV/c reported in Ref. 4, in which this distance varied between 120 and 180 in.)

The target-full and target-empty trigger rates were 1.0×10^{-4} and 0.16×10^{-4} trigger per incident pion, respectively. There were 33 000 target-full and 2000 target-empty pictures taken; 37% of these contained 2γ events.

III. ANALYSIS

A. Scanning, Measuring, and Fiducial Region

All of the pictures were scanned twice for 2γ events, and any discrepancies between the two scans were resolved by a third look at the events in question. The first spark of each shower was encoded in each of the 90° stereo views. The γ angles were calculated, using the approximation that each event originated at the center of the hydrogen target. This set the maximum error in the γ-γ opening angle as $\pm$(half-length of hydrogen target)/(distance from hydrogen target to spark chamber), i.e., $\pm1.7\%$ for the low-energy run and $\pm6.4\%$ for the 10-GeV/c run.

Events were accepted only if both γ's originated in the brass plates of the spark chamber within ±11 in. from the beam axis, converted before the last four plates, and had a minimum of three gaps firing per γ ray.

B. Opening-Angle Distributions

1. Experimental Distributions

Several γ-γ opening-angle distributions in the π^-p c.m. system are shown in Fig. 2. The 2.9-GeV/c distribution is typical of all momenta in the 2.4- to 3.8-GeV/c range. The opening angle θ between two γ's has a minimum allowed value $\theta_{\min}$ determined by

$$\tan\tfrac{1}{2}\theta_{\min}=mc/p\,, \qquad (4)$$

where m and p are the mass and momentum of the particle decaying into two γ's (either π^0 or η^0). The opening-angle distributions are plotted normalized to $\theta_{\min}$, and should peak sharply at the minimum value of $\theta/\theta_{\min}=1.0$. The smoothing out of the leading edge of these distributions is due to the uncertainty in the γ-γ opening-angle measurement and to the spread in incident beam momentum.

The opening-angle spectra have been corrected for the target-empty background. Over essentially the full range of $\theta/\theta_{\min}$ values 0.5 to 6.0, this amounts typically to a 40% subtraction in the low-energy region and 13% at 10 GeV/c.

2. Cut in Distributions

Only those events in the interval $0.965\leq\theta/\theta_{\min}$ ≤1.165, which includes about half of the good events,

[29] W. Galbraith, E. W. Jenkins, T. F. Kycia, B. A. Leontic, R. H. Phillips, A. L. Read, and R. Rubinstein, Phys. Rev. 138, B913 (1965).

are used in determining the differential charge-exchange cross sections. This narrow cut is made for three reasons: (1) The target-empty subtraction in this narrow interval is much lower: typically 20% in the lower-energy region and 8% at 10 GeV/c. (2) The inelastic contamination from $m\gamma$ events ($m\geq 3$), where only two out of the m γ's have appeared in the spark chamber, is reduced to a negligible level (except for η^0 events at 10 GeV/c). (3) The third and most important reason is that this narrow cut improves the resolution in the measurement of the π^0 angular distributions. The observed variable is the bisector of the γ's; the narrower the opening-angle interval selected, the closer the bisector is to the true π^0 direction and the smaller the uncertainty in the π^0 direction. Good angular resolution is essential for a reasonable estimation of the forward differential cross section.

To give an absolute measure of this cut in $\theta/\theta_{\min}$ at an incident π^- momentum of 3 GeV/c, the c.m. momentum of the π^- is 1.10 GeV/c, and this is the same as the π^0 momentum for the charge-exchange reaction. Using Eq. (4), $\theta_{\min}=14.0°$ in the π^-p c.m. system, and the cut in θ is from 13.5° to 16.3°. Thus the cut includes only 2.8° out of the total of 166.5° in the allowed $13.5°<\theta<180°$ range.

To determine exactly what fraction of the charge-exchange events are included within this opening-angle cut, a Monte Carlo calculation is made to predict the expected $\theta/\theta_{\min}$ distribution. These Monte Carlo results are shown as solid curves in Fig. 2; the agreement in shape with the experimental histograms is good.

3. Check on Beam Momentum

Besides being necessary for the normalization determination, the comparisons of these Monte Carlo opening-angle distributions with the experimental distributions provide a check on the incident beam momentum and point out the presence of inelastic backgrounds. The incident-beam-momentum check is accomplished by comparing the positions of the peaks of the $\theta/\theta_{\min}$ distributions. The location of this peak depends upon

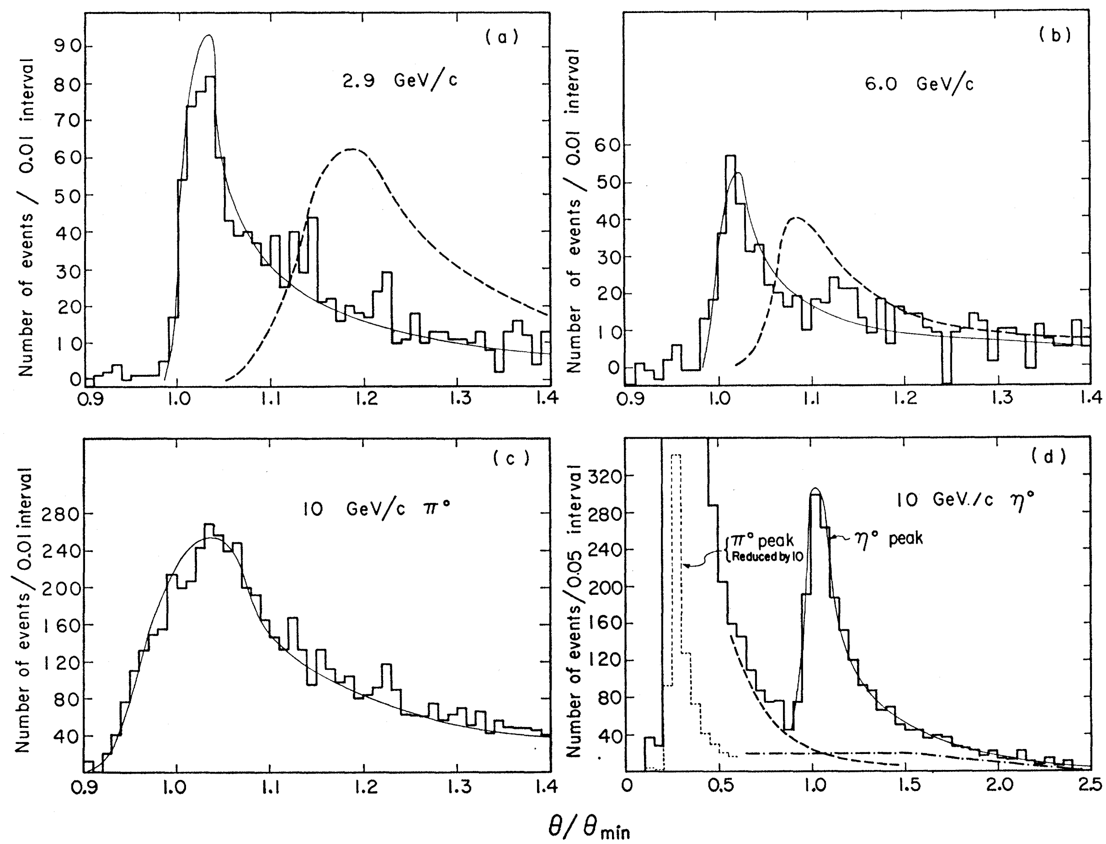

FIG. 2. Distributions of the 2γ opening angles θ in the π^-p c.m. system, normalized to the minimum allowed opening angle $\theta_{\min}$ for each momentum. Note that the sharpness in the opening-angle distribution is masked here by the expanded scale and buried zero in $\theta/\theta_{\min}$ (see text for absolute angular scale). The solid lines are the Monte Carlo predicted distributions, normalized to the number of experimental events in the interval $0.965\leq\theta/\theta_{\min}\leq 1.165$. The dashed lines in (a) and (b) are the Monte Carlo predicted distributions for the π^0 in the reaction $\pi^-+p\rightarrow N^{*0}(1236)+\pi^0$, and are arbitrarily normalized. (a) The 2.9-GeV/c distribution is typical of all those between 2.4 and 3.8 GeV/c. (d) The η^0 $\theta/\theta_{\min}$ distribution has two backgrounds (see text)—the tail of the π^0 distribution which extends under the η^0 peak (dashed line) and a residual flat background from multi-γ events (shown by dash-dot line). The η^0 Monte Carlo calculated distribution (solid line) includes these two backgrounds.

the beam momentum via the calculation of $\theta_{\min}$, using Eq. (4). We observed a 1.5% displacement of the Monte Carlo peaks relative to the experimental peaks for all of the 2.4–3.8-GeV/c distributions, a 1% displacement at 6 GeV/c, and no displacement at 10 GeV/c. The Monte Carlo curves in Fig. 2 have been shifted by these amounts. There are two other possible sources of this shift: an error in the measurement of the distance between the hydrogen target and the spark chamber, or an error in the measurement of the distance between the reference marks in the spark-chamber pictures. Either of these would produce an error in θ.

Upon rechecking, an error of 0.9% was discovered in the hydrogen-target-to-spark-chamber distance in the low-energy run, which accounts for a 0.9% shift in the experimental determination of θ. This leaves only a 0.6% shift. Instead of reanalyzing all the data after this 0.9% error was discovered, the Monte Carlo curves were simply shifted over as stated above, allowing the correct calculation of the number of events surviving the opening-angle cut.

Our best estimate for the experimental uncertainty in θ because of errors in distance measurements is $\pm 0.6\%$. The best estimate for the experimental uncertainty in $\theta/\theta_{\min}$ because of errors in the beam-momentum measurement is $\pm 0.6\%$. The combined error in $\theta/\theta_{\min}$ is $\pm 0.8\%$. Thus the 0.6% shift is within our experimental uncertainty, and the value of the momentum of the incident beam is verified to this accuracy.

4. *Isobar Contamination*

The most likely source of contamination in our charge-exchange data is nucleon-isobar production:

$$\pi^- + p \rightarrow N^{*0} + \pi^0, \quad N^{*0} \rightarrow n + \pi^0, \tag{5}$$

with the fairly low-energy γ's from the isobar's π^0 failing to trigger the anticoincidence system. The opening-angle distributions for this reaction have been calculated with a similar Monte Carlo program, which simulates N^* production and decay according to the isobaric model and takes into account the energy dependence of the γ-detection efficiency of the anticoincidence system. The dashed lines in Figs. 2(a) and 2(b) show these distributions for the $N^*(1238)$ isobar. All higher-mass isobars would produce an opening-angle peak shifted considerably farther to the right and have a negligible contribution to the data.

The comparison of the Monte Carlo curves with the experimental histograms in Figs. 2(a) and 2(b) shows that the isobar contamination is small, especially within the $\theta/\theta_{\min}$ interval from 0.965 to 1.165. A least-squares fit of the experimental data to the Monte Carlo elastic and isobar distributions gives an average isobar contamination of 4% in the 2.4–3.8-GeV/c data. However, since the χ^2 value for zero isobar contamination is almost as low as the minimum χ^2 value corresponding to the 4% contamination, the data are consistent with zero isobar contamination, and we have not corrected for it in our normalizations.

C. Bisector-to-π^0 Conversion

The experimentally observed differential-scattering variable is the direction of the bisector of the two γ's which is not the same as the true π^0 direction. But because of the narrow cut accepted in the opening-angle distributions, $0.965 \leq \theta/\theta_{\min} \leq 1.165$, the bisector direction is usually a good approximation to the π^0 direction, and the t dependence (t is the square of the four-momentum transfer to the nucleon) of the π^0 and bisector distributions are quite similar.

If the π^0 distribution in t were known, it would be possible to predict the bisector distribution (statistically), knowing that the spinless pion decays isotropically in its rest system. Denoting the π^0 distribution by $P(t)$ and the bisector distribution by $B(t)$, we can express their relationship for any t interval t_i as

$$B(t_i) = \epsilon(t_i) P(t_i), \tag{6}$$

where $\epsilon(t_i)$ is the efficiency factor for the ith t interval. Ideally, then, the π^0 distribution can be determined by inverting this equation:

$$P(t_i) = w(t_i) B(t_i), \tag{7}$$

where $w(t_i) = 1/\epsilon(t_i)$ is the weight for the ith interval.

Unfortunately, such a method requires an *a priori* knowledge of the true π^0 distribution, because the values of the weights depend upon the shape of the π^0 distribution. Accordingly, the weights used here were determined by finding a π^0 distribution which produces a bisector distribution in reasonable agreement with the observed bisector distribution. This was done in the following way.

Let the probability of a π^0 in t-interval j producing a bisector in t-interval i be denoted by A_{ij}. These A_{ij} are determined by using a Monte Carlo calculation, and will be discussed further below. Then

$$B(t_i) = \sum_j A_{ij} P(t_j). \tag{8}$$

Expanding the π^0 distribution in powers of t,

$$P(t) = \sum_{n=0}^{n_{\max}} a_n t^n, \tag{9}$$

gives

$$B(t_i) = \sum_{n=0}^{n_{\max}} a_n \sum_j A_{ij} t_j^n. \tag{10}$$

Using a least-squares fit of these $B(t_i)$ to the experimental bisector distribution, the values of a_n (and thus the best-fit π^0 distribution) were calculated for $n_{\max} = 2$ through $n_{\max} = 8$. The weights $w(t_i) = P(t_i)/B(t_i)$ were also calculated for each value of $n_{\max}$. In general, the best value of $n_{\max}$ was chosen as that which produced the lowest value of χ^2/f, where f is the number of degrees of freedom in the least-squares fit. The weights for this best value of $n_{\max}$ were inserted into Eq. (7), giving the best estimate of the π^0 distribution. Even though the values of the a_n varied considerably as a function of the value of $n_{\max}$, the values of the weights were relatively insensitive to the value of $n_{\max}$. This procedure was used independently for each value of the incident momentum, and also for η^0's at 10 GeV/c.

The A_{ij} matrix as calculated with the Monte Carlo program includes the effects of (a) the finite beam size, (b) the momentum spread of the beam, (c) the length of the hydrogen target, and (d) the conversion distribution by gaps of the γ's converting in the spark chamber. It also includes corrections for (a) fraction of events outside of the $0.965\leq\theta/\theta_{\min}\leq1.165$ opening-angle cut (about $\frac{1}{2}$), (b) events lost because of conversion of recoil neutrons in the scintillators surrounding the hydrogen target ($\sim3\%$ average effect), (c) events lost because of conversion of γ's in the stainless-steel side walls of the hydrogen target and its vacuum jacket ($\lesssim1\%$ average effect), (d) events lost because of passage of γ's through the beam hole in the large scintillator downstream from the spark chamber (negligible at and below 6 GeV/c; not applicable at 10 GeV/c), (e) events lost because of passage of γ's through the spark chamber without converting (3.8% per γ ray), and (f) events lost because of scattering of γ's outside the region defined by the spark chamber (causes cutoff of t distribution except at 6 and 10 GeV/c). Corrections (b), (c), (d), and (f) are included here in the A_{ij} calculation because they are t-dependent and must properly be applied to the π^0 (or η^0) distribution rather than the bisector distribution. Corrections (a) and (e) are included here for convenience, although they could just as properly be included in the over-all normalization factors.

The only correction applied to the raw bisector distribution was the target-empty subtraction, which has been described above. This subtraction was made, using the t distribution of the empty-target events.

D. Over-All Normalization Corrections

These corrections are called "over-all" to distinguish them from the t-dependent corrections just discussed above. They include (a) μ contamination of beam (typically $\sim5\%$), (b) K contamination of beam (typically $\sim2\%$, except none at 10 GeV/c), (c) absorption of beam in hydrogen target ($<1\%$), (d) δ rays in hydrogen target ($\sim1\%$), (e) Dalitz pairs ($\sim1\%$), (f) γ conversion before spark chamber (3.1% per γ ray), (g) scanning inefficiency ($\sim1\%$), (h) mismeasured events (typically $\sim4\%$), and (i) pictures with events accompanied by three or more unassociated charged tracks ($\sim1\%$).

In addition, there are two corrections applied only to the η^0 distribution at 10 GeV/c. The first is caused by a background of π^0 events. This is evident from the $\theta/\theta_{\min}$ distribution shown in Fig. 2(d), where the tail of the π^0 distribution is seen to extend into the region of the η^0 peak. This π^0 background is estimated to be $\sim8\%$. It is subtracted bin by bin in the η^0 t distribution, using the t distribution of the π^0 events. The necessity for a second correction can also be seen from Fig. 2(d). After the π^0 events have been subtracted, there is still a background under the η^0 $\theta/\theta_{\min}$ peak. This background is essentially flat in $\theta/\theta_{\min}$. It is presumably because of events in which three or more γ's were produced, but only two γ's were observed. This amounts to a background of $\sim10\%$, and is corrected for in the over-all normalization factor.

E. Systematic Errors

The systematic uncertainties in the over-all cross-section measurements are estimated to be $\pm10\%$ for the 2.4–6.0-GeV/c data, $\pm8\%$ for the π^0 data at 10 GeV/c, and $\pm11\%$ for the η^0 data at 10 GeV/c. For any given momentum, the systematic errors from point to point in the t distributions are negligible compared to the statistical errors. Also, for the 2.4–3.8-GeV/c data, the systematic errors from momentum to momentum are negligible compared to the statistical errors. The major contributions to the systematic errors arise from the uncertainties in the number of protons/cm^2 in the hydrogen target and the μ contamination of the beam. The presence of a possible small isobar contamination is not included in the systematic error; as described above, the data are consistent with zero contamination. As a precaution against introducing systematic errors between the data at different momenta, during the 2.4–3.8-GeV/c run most of the data were taken in sets of 500 pictures at each momentum, running back and forth many times over the whole momentum interval.

IV. RESULTS AND CONCLUSIONS

A. 2.4- to 3.8-GeV/c Data

The differential π^0 distributions between 2.4 and 3.8 GeV/c are summarized in Table I and plotted in Figs. 3 and 4. Only statistical errors are included in these data; the systematic errors are described in Sec. III. These values for $d\sigma/dt$ near $t=0$ differ from those given in the preliminary results[1] by somewhat more than would be expected on the basis of statistics alone. The reasons for these differences were studied and found to be twofold: (i) an overestimated initial scanning efficiency for the once-scanned preliminary data and (ii) fluctuations in the small numbers of empty-target events.

The maximum observable scattering angle is set by the size of the spark chamber and its distance from the hydrogen target. These were fixed during the 2.4–6.0-

TABLE I. Values of the differential cross section $d\sigma/dt$ in μb/(GeV/c)^2 for the charge-exchange reaction $\pi^- + p \rightarrow \pi^0 + n$.

$-t$ interval [(GeV/c)^2]	Incident pion lab momentum (GeV/c) 2.4	2.5	2.6	2.8	2.9	3.0
0.00–0.01	690±180	270±170	700±140	780±170	1250±180	1280±210
0.01–0.03	870±200	630±200	1100±130	1170±110	1070±130	850±150
0.03–0.06	1230±150	1000±150	1150±110	1040±110	1110±110	1050±110
0.06–0.09	990±160	820±170	1140±120	1090±100	1130±100	1120±120
0.09–0.13	1160±150	980±130	1000± 90	860± 90	770± 80	790± 90
0.13–0.18		670±130	600± 90	570± 70	620± 60	600± 70
0.18–0.23					490± 70	460± 60
0.23–0.29						
Number of events	319	380	1504	1779	1179	781

	3.1	3.2	3.3	3.4	3.5	3.6	3.8
0.00–0.01	1340±190	1110±190	630±160	420±150	260±140	200±170	800±190
0.01–0.03	1020±140	860±140	790±140	520±120	570±140	440±150	790±130
0.03–0.06	1050±110	930±110	1060±100	830±110	890±110	700±110	500±120
0.06–0.09	980±100	730±100	930±110	940±120	900±100	810±100	600±110
0.09–0.13	770± 80	700± 90	650± 80	710± 90	880± 90	750± 90	660± 90
0.13–0.18	590± 60	560± 70	510± 60	520± 70	490± 60	520± 70	360± 60
0.18–0.23	430± 60	390± 60	310± 50	310± 60	320± 60	490± 50	260± 50
0.23–0.29						240± 40	170± 40
Number of events	924	694	888	447	687	674	471

GeV/c run, and hence the maximum t value increases with the incident momentum. The total numbers of events given in Tables I and II are the numbers remaining after the target-empty subtraction and the 0.965-to-1.165 cut in $\theta/\theta_{\min}$.

The resolution in t decreases as a function of t. The data are plotted in t intervals which closely approximate

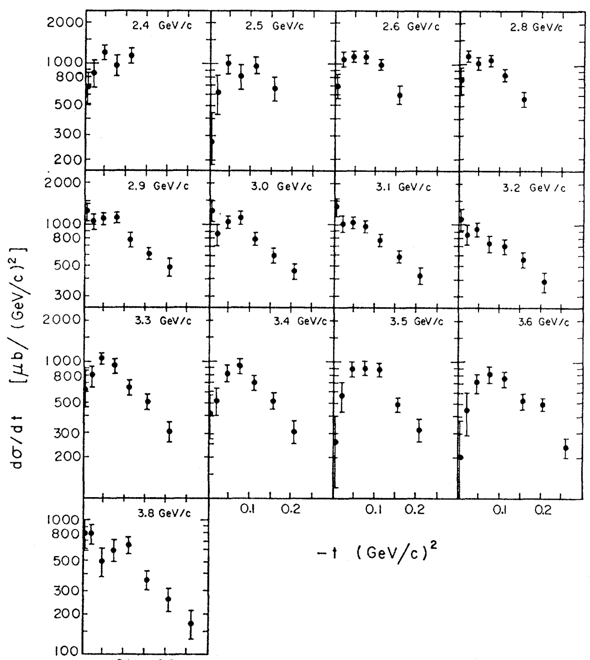

FIG. 3. The differential $\pi^- + p \rightarrow \pi^0 + n$ charge-exchange cross sections between 2.4 and 3.8 GeV/c plotted versus the square of the four-momentum transfer to the nucleon t. The errors shown are statistical only. The systematic uncertainty for the data as a whole is ±10%, but does not affect the relative normalizations for the different momenta.

the average resolution in t over the 2.4–3.8-GeV/c momentum range. This can be expressed quantitatively in the following way. If π^0's were produced isotropically across one of the t intervals, approximately $\frac{2}{3}$ of the resulting bisectors of the γ's would fall into the same t interval.

These t distributions in Fig. 3 appear to consist of two qualitatively distinct regions. The first consists of the data for $|t| \gtrsim 0.08$ (GeV/c)^2, where the differential cross section falls off roughly exponentially, and the shape is nearly the same for all momenta; such behavior is quite similar to the higher-energy charge-exchange scattering.[4,10] The second region, for $|t| \lesssim 0.08$(GeV/c)^2, shows a rapidly varying shape as a function of momentum, sometimes dipping and sometimes peaking at $t=0$.

These momentum-dependent effects can be seen clearly in Fig. 4, where $d\sigma/dt$ is plotted as a function of the incident pion lab momentum p. Because of the fairly narrow momentum interval covered by these data, the appearance of Fig. 4 would be essentially unchanged whether presented as a semilog or log-log plot; a semilog scale is used for convenience. Nearest the forward direction, at $-t=0.005$ (GeV/c)^2, $d\sigma/dt$ shows sharp minima at 2.5 and 3.6 GeV/c and a maximum at 3.0 GeV/c. At larger values of $|t|$, the distributions become much smoother, in general decreasing gradually as a function of p.

Approximate values of the real part of the forward charge-exchange amplitude A_{ex} can be calculated using $d\sigma/dt$ ($t \approx 0$) and the differences in the $\pi^{\pm}p$ total cross sections $\Delta\sigma = \sigma^- - \sigma^+$:

$$[\mathrm{Re}A_{\text{ex}}\,(t=0)]^2 = d\sigma/dt\,(t=0) - [\mathrm{Im}A_{\text{ex}}\,(t=0)]^2, \quad (11)$$

where

$$4\pi h\,\mathrm{Im}A_{\text{ex}}\,(t=0) = \Delta\sigma(\tfrac{1}{2}\pi)^{1/2}. \quad (12)$$

Using the value of $d\sigma/dt$ for the first t interval $0 \leq |t|$

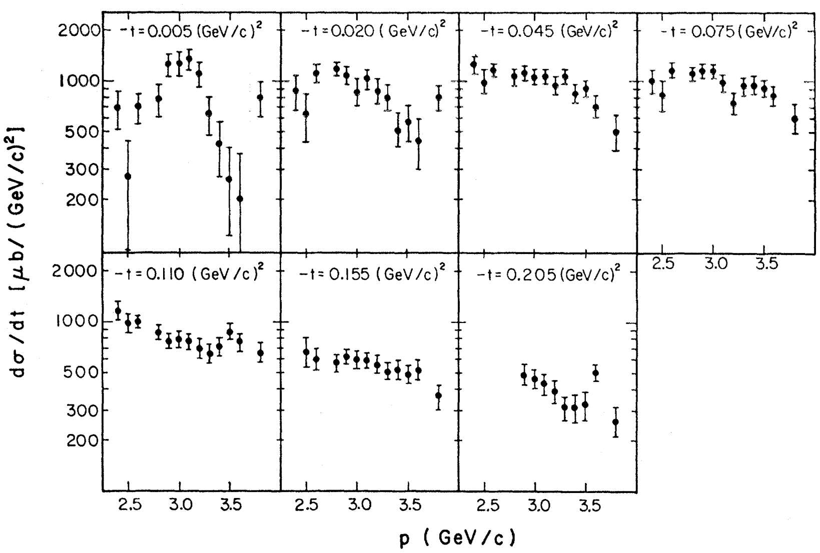

FIG. 4. The differential $\pi^- + p \to \pi^0 + n$ charge-exchange cross section at fixed t plotted versus the incident pion lab momentum p.

≤ 0.01 (GeV/c)^2 as an approximation to $d\sigma/dt$ ($t=0$), and the total cross sections of Citron *et al.*,[28] the real parts of the forward amplitude are calculated in Table II.

A plot of the complex charge-exchange amplitude as a function of incident momentum is a convenient method of displaying resonant structure. Following the method and terminology of Höhler *et al.*,[21,30] and using natural units ($\hbar = m_{\pi^+} = c = 1$),

$$\frac{d\sigma_{\mathrm{ex}}}{d\Omega_{\mathrm{c.m.}}}(0^\circ) = \frac{q^2}{\pi}\frac{d\sigma_{\mathrm{ex}}}{dt}(t=0) = |F_{\mathrm{ex}}(0^\circ)|^2 = 2|F_b^{(-)}|^2, \quad (13)$$

$$\mathrm{Im}F_b^{(-)} = q\Delta\sigma/8\pi, \quad (14)$$

and

$$[\mathrm{Re}F_b^{(-)}]^2 = \tfrac{1}{2}\frac{d\sigma_{\mathrm{ex}}}{d\Omega_{\mathrm{c.m.}}}(0^\circ) - [\mathrm{Im}F_b^{(-)}]^2, \quad (15)$$

where q is the pion momentum in the c.m. system.

The values of $q\,\mathrm{Im}F_b^{(-)}$ and $q|\mathrm{Re}F_b^{(-)}|$ are given in Table II and plotted in Fig. 5. The variable $qF_b^{(-)}$ should execute a counterclockwise circle when passing through an elastic resonance. Distortions of these circles can be the results of overlapping resonances or of energy-dependent inelasticity or background factors. The counterclockwise excursions of the amplitude in Fig. 5 are quite similar to those demonstrated by the lower-energy resonances below 2.5 GeV/c.[21,30] The error in $d\sigma/dt$ ($t=0$) gives rise to an error in the dis-

TABLE II. Calculated values of the real part of the forward charge-exchange amplitude, using the measured values of $d\sigma/dt$ near the forward direction $0 \leq |t| \leq 0.01$ (GeV/c)^2 and the total-cross-section values of Citron *et al.*[a] Systematic as well as statistical errors are included.

p (GeV/c)	$\Delta\sigma$[a] (mb)	$\mathrm{Im}A_{\mathrm{ex}}$ ($t=0$) (10^{-15} cm/(GeV/c))	$\lvert\mathrm{Re}A_{\mathrm{ex}}$ ($t=0$)$\rvert$ (10^{-15} cm/(GeV/c))	$d\sigma_{\mathrm{ex}}/d\Omega_{\mathrm{c.m.}}(0^\circ)$ (μb/sr)	$q\lvert F_b^{(-)}\rvert$ (natural units)[b]	$q\,\mathrm{Im}F_b^{(-)}$ (natural units)[b]	$q\lvert\mathrm{Re}F_b^{(-)}\rvert$ (natural units)[b]
2.5	3.29±0.22	16.6±1.1	0	86±54	0.33±0.10	0.34±0.02	0
2.6	2.64±0.22	13.3±1.1	23±4	232±53	0.56±0.07	0.28±0.02	0.48±0.08
2.8	2.61±0.22	13.2±1.1	25±4	279±68	0.64±0.08	0.30±0.03	0.56±0.09
2.9	2.89±0.22	14.6±1.1	32±4	464±82	0.83±0.08	0.35±0.03	0.76±0.09
3.0	3.24±0.22	16.4±1.1	32±4	493±96	0.88±0.08	0.40±0.03	0.78±0.09
3.1	3.47±0.22	17.5±1.1	32±4	535±92	0.93±0.08	0.45±0.03	0.81±0.09
3.2	3.58±0.22	18.1±1.1	28±4	459±91	0.88±0.09	0.48±0.03	0.74±0.11
3.3	3.57±0.22	18.0±1.1	17±5	270±73	0.68±0.09	0.49±0.03	0.48±0.14
3.4	3.43±0.22	17.3±1.1	11±7	186±71	0.58±0.11	0.49±0.03	0.31±0.22
3.5	3.35±0.22	16.9±1.1	0	119±64	0.47±0.13	0.49±0.03	0
3.6	3.15±0.22	15.9±1.1	0	95±81	0.43±0.18	0.48±0.03	0
3.8	2.91±0.22	14.7±1.1	24±4	404±106	0.91±0.12	0.47±0.04	0.78±0.14

[a] Reference 28.
[b] ($\hbar = m_\pi = c = 1$).

[30] G. Höhler, J. Baacke, J. Giesecke, and N. Zovko, Proc. Roy. Soc. (London) **A289**, 500 (1966).

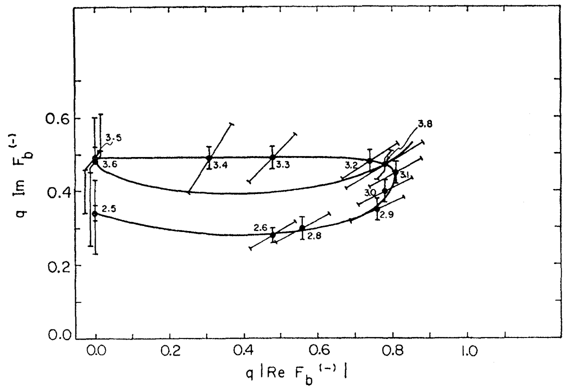

FIG. 5. Complex diagram of the forward charge-exchange amplitude $qF_b^{(-)}$ where q is the pion c.m. momentum and $d\sigma_{ex}/d\Omega_{c.m.}(0^0)=2|F_b^{(-)}|^2$. Each point is labeled by the corresponding incident pion lab momentum in GeV/c. Natural units are used for $qF_b^{(-)}$ ($\hbar=m_{\pi^+}=c=1$). The curve is drawn free-hand as a guide.

tance from the origin $q|F_b^{(-)}|$, and the error in $\Delta\sigma$ gives the error in $q\,\mathrm{Im}F_b^{(-)}$; all errors include systematic as well as statistical errors.

Figure 5 shows a qualitative similarity to the momentum dependence of the forward charge-exchange amplitude as calculated by Höhler *et al.*[21,30] in this energy region, using the optical theorem and dispersion relations. Quantitatively, the variations in the real part of the amplitude are considerably greater than those calculated by Höhler *et al.* However, it should be reiterated that these values of the real parts are only approximate, owing to the poor statistics on $d\sigma/dt$ at $-t=0.005$ (GeV/c)^2, as well as the uncertainty in extrapolating $d\sigma/dt$ from $-t=0.005$ (GeV/c)^2 to $t=0$.

It seems apparent that whether or not a Regge-type mechanism is used to explain the exponential falloff for $|t|\gtrsim 0.08$ (GeV/c)^2, the small-t behavior of the differential cross section in this energy region is still dominated by the N^* resonances. As pointed out in Ref. 1 and mentioned above in the Introduction, the 2.5-GeV/c minimum, the 3.0-GeV/c maximum, and the 3.6-GeV/c minimum in $d\sigma/dt$ ($t\approx 0$) are consequences of the presence of the $N_{3/2}^*(2420)$, the $N_{1/2}^*$ (2650), and the $N_{3/2}^*(2850)$ resonances, respectively.

The only other experiment with comparable t resolution is that of the Saclay-Orsay group between 2.6 and 5.8 GeV/c. A sample of their data appears in Ref. 24, in particular, a plot of $d\sigma/dt$ versus p for the fixed-t interval $0\leq|t|\leq 0.01$ (GeV/c)^2, which may be compared to the data shown in Table I and Fig. 4 for the same t interval. The average value of $d\sigma/dt$ and the qualitative shape of the $d\sigma/dt$-versus-p curve (in the sense of locations of minima and maxima of $d\sigma/dt$) are in good agreement for the two sets of data, but the data presented here show a much higher maximum and much lower minima than those of Ref. 24. Even allowing for the poorer statistics of our data, we believe that the sharpness of our maximum and minima is due to a better resolution in t near $t=0$; this increased resolution is due to the physical fact that the hydrogen-target-to-spark-chamber distance was considerably greater in our experimental setup than was the corresponding distance for the experimental arrangement of the Saclay-Orsay group.

A further comparison can be made between the differential cross section at 3.9 GeV/c shown in Ref. 24 and that at 3.8 GeV/c given here in Table I and Fig. 3. There is good agreement, within statistics, over the common range in t. The Saclay-Orsay data have the advantage of better statistics and a much wider range in t.

B. 6- and 10-GeV/c Data

The differential-scattering distributions for the 6- and 10-GeV/c data are summarized in Table III and plotted in Figs. 6–8. The η^0 cross sections refer to the

TABLE III. Values of the differential cross section $d\sigma/dt$ in μb/(GeV/c)^2 for the pion charge-exchange reaction $\pi^-+p\to\pi^0+n$ at 6 and 10 GeV/c, and for the η production reaction $\pi^-+p\to\eta^0+n$ at 10 GeV/c. The η^0 cross sections are for the 2γ decay mode only.

π^0 at 6 GeV/c		π^0 at 10 GeV/c		η^0 at 10 GeV/c	
$-t$ interval [(GeV/c)^2]	$d\sigma/dt$ [μb/(GeV/c)^2]	$-t$ interval [(GeV/c)^2]	$d\sigma/dt$ [μb/(GeV/c)^2]	$-t$ interval [(GeV/c)^2]	$d\sigma/dt$ [μb/(GeV/c)^2]
0.00–0.04	382±64	0.00–0.08	230 ±7	0.00–0.12	17.9 ±1.8
0.04–0.08	402±59	0.08–0.16	163 ±6	0.12–0.24	20.6 ±1.8
0.08–0.14	252±46	0.16–0.24	89 ±4	0.24–0.36	18.2 ±1.6
0.14–0.20	194±39	0.24–0.36	37 ±3	0.36–0.56	10.3 ±0.9
0.20–0.28	124±26	0.36–0.52	9 ±2	0.56–0.84	3.8 ±0.5
0.28–0.38	40±16	0.52–0.72	0.6±0.6	0.84–1.20	0.91±0.23
0.38–0.50	17±8	0.72–0.96	2.6±0.5	1.20–1.68	0.23±0.12
0.50–0.62	2±4	0.96–1.24	3.3±0.5	1.68–2.28	0.24±0.12
0.62–0.76	10±7	1.24–1.56	1.0±0.3		
0.76–0.90	10±6	1.56–1.92	0.4±0.2		
		1.92–2.32	0.2±0.2		
$\int_0^{-0.9}\frac{d\sigma}{dt}dt$ (μb)	77±10	$\int_0^{-2.32}\frac{d\sigma}{dt}dt$ (μb)	46.6±3.8	$\int_0^{-2.28}\frac{d\sigma}{dt}dt$ (μb)	10.5 ±1.2
Number of events	440	Number of events	3685	Number of events	869

2γ decay mode only, and so they must be divided by the 2γ branching ratio if the total η^0 cross sections are desired. The differential cross sections include statistical errors only, whereas the integrated cross sections include systematic as well as statistical errors. These systematic errors are described above.

The resolution in t at 6 GeV/c is approximately the same as the interval widths used in plotting the data, just as described above for the 2.4–3.8-GeV/c data. At 10 GeV/c, this criterion is relaxed somewhat, the plotted interval widths being a little narrower than the resolution in t. This is justified to some extent by the large statistics in the intervals near the forward direction. For the 10-GeV/c π^0's, the resolution in t varies from $\Delta t=0.04$ at $-t=0.02$, to $\Delta t=0.20$ at $-t=0.50$, to $\Delta t=0.40$ at $-t=1.60$; all units are in

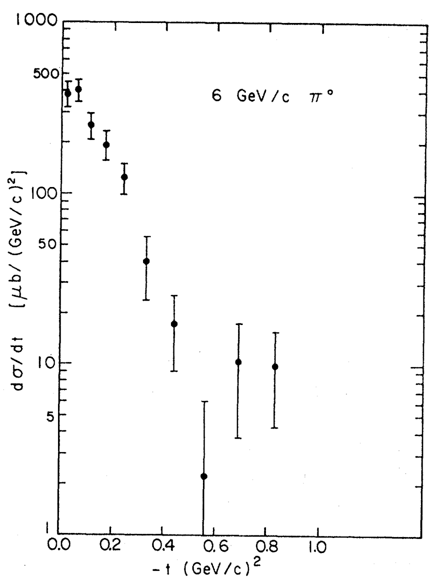

FIG. 6. The differential $\pi^-+p\rightarrow\pi^0+n$ charge-exchange cross section at 6 GeV/c.

(GeV/c)^2. For the 10-GeV/c η^0's, the resolution in t varies from $\Delta t=0.12$ at $-t=0.06$, to $\Delta t=0.40$ at $-t=0.50$, to $\Delta t=0.68$ at $-t=1.60$.

Both the 6- and 10-GeV/c π^0 distributions show the same features, which by now are well established[2,4,10,11]: the slight turnover at small values of t, the exponential falloff with a slope of $\sim$10 (GeV/c)$^{-2}$, the minimum near $-t=0.6$ (GeV/c)^2, and a second maximum near $-t=1.0$ (GeV/c)^2. Our data at 6 and 10 GeV/c reported in Ref. 4 are more accurate at small t values than the data presented here; these data serve the purpose of an extension of the distributions out to larger t values.

The 10-GeV/c η^0 distribution is similar to the π^0 distributions as far as having a slight turnover near $t=0$ and an exponential falloff at larger values of t,

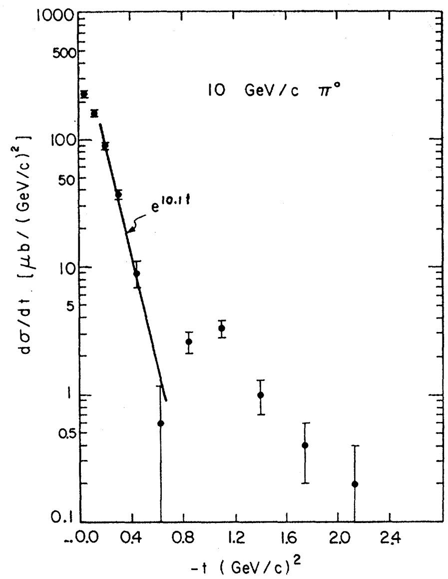

FIG. 7. The differential $\pi^-+p\rightarrow\pi^0+n$ charge-exchange cross section at 10 GeV/c. The straight line is a fit-by-eye to the exponential slope.

but the exponential slope is only $\sim$4 (GeV/c)$^{-2}$, much flatter than the π^0 slope.

A detailed comparison is given in Table IV of these π^0 and η^0 results with those of the Saclay-Orsay group[10,11,17] and with those of our previously reported high-energy run[4] [see Sec. I, item (B) above; these early data are completely independent of the data reported here]. These values include systematic as well as statistical errors. In general, these three sets of data are in good

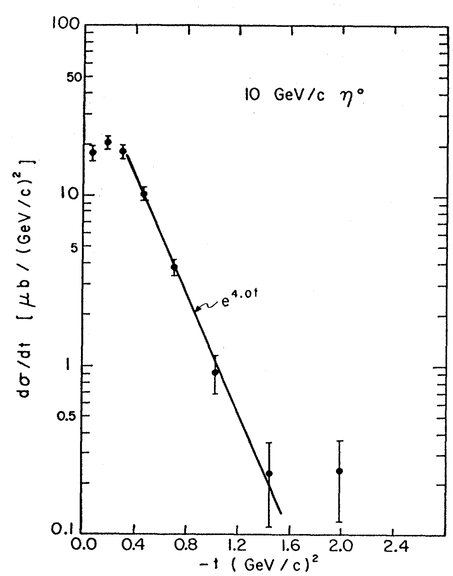

FIG. 8. The differential η-production cross section $\pi^-+p\rightarrow\eta^0+n$ at 10 GeV/c. The η^0 cross sections are for the 2γ decay mode only. The straight line is a fit-by-eye to the exponential slope.

TABLE IV. Comparison of the values of $d\sigma/dt$ near $t=0$ and the integrated cross sections with the results of our high-energy small-angle run (Ref. 4) and with the results of the Saclay-Orsay collaboration (Refs. 10, 11, and 17). The η^0 cross sections are for the 2γ decay mode only.

	Our previous data at small angles	Saclay-Orsay collaboration	Present data
6 GeV/c, π^0			
$\frac{d\sigma}{dt}$ $(-t=0$ to $0.04)$	333 ± 41 μb/(GeV/c)^2	402 ± 22 μb/(GeV/c)^2	382 ± 75 μb/(GeV/c)^2
$\int_0^{-0.4}\frac{d\sigma}{dt}dt$	74 ± 7 μb	83 ± 4 μb	72 ± 9 μb
$\int_0^{-0.9}\frac{d\sigma}{dt}dt$		87 ± 4 μb	77 ± 10 μb
10 GeV/c, π^0			
$\frac{d\sigma}{dt}$ $(-t=0$ to $0.08)$	222 ± 23 μb/(GeV/c)^2	237 ± 13 μb/(GeV/c)^2	230 ± 20 μb/(GeV/c)^2
$\int_0^{-0.4}\frac{d\sigma}{dt}dt$	48.6 ± 4.3 μb	45 ± 2.5 μb	43 ± 3.6 μb
10 GeV/c, η^0			
$\frac{d\sigma}{dt}$ $(-t=0$ to $0.12)$		25.1 ± 3.5 μb/(GeV/c)^2	17.9 ± 2.7 μb/(GeV/c)^2
$\int_0^{-0.7}\frac{d\sigma}{dt}dt$		9.7 ± 1.2 μb	9.4 ± 1.1 μb

agreement. In addition, the best by-eye fits to our exponential slopes are $e^{10.1t}$ and $e^{4.0t}$ for the 10-GeV/c π^0 and η^0 distributions, respectively. These agree very well with the corresponding best-fit slopes of the Saclay-Orsay group,[10,17] namely, $e^{(10.5\pm0.4)t}$ and $e^{(4.0\pm1.2)t}$.

ACKNOWLEDGMENTS

A large number of people have contributed to various parts of this experiment. We would like to thank especially L. Sodickson, who contributed in great measure to both the running of the experiment and the early stages of the data analysis, and also O. Fackler, E. Shibata, L. Stinson, and C. Ward, who were indispensible in the running of the experiment. A. Buffington, T. Kan, J. Kasper, P. Kirk, T. Lyons, M. Poe, S. Smith, L. Sompayrac, and C. Strumski also assisted during the experimental run. A. Bigi, R. Carrara, R. Casali, and especially F. Sergiampietri contributed to the analysis calculations. We thank E. Bonis for organizing and keeping track of the large amount of data scanning, measuring, and handling, and the MIT scanning group for their diligent work. We are especially indebted to Professor D. Frisch for his advice and support throughout the experiment. Many interesting discussions with P. Mockett proved to be very helpful. In particular, it was his suggestion to study the pion-nucleon resonant structure between 2 and 4 GeV/c, using the forward charge-exchange scattering as a measure of $\sigma^- - \sigma^+$ (the difference between the $\pi^- p$ and $\pi^+ p$ total cross sections), which largely initiated the low-energy run in this experiment. We would like to acknowledge the hospitality and assistance of the Brookhaven National Laboratory and its staff during the experimental run at the AGS. One of us (IM) would also like to acknowledge greatly the hospitality and financial assistance of the MIT Laboratory for Nuclear Science and the Brookhaven National Laboratory. Computer calculations have been carried out using the 7044 of the MIT Laboratory for Nuclear Science and the CNUCE 7090 at Pisa.